Formation of helical beams by use of Pancharatnam–Berry phase optical elements

Gabriel Biener, Avi Niv, Vladimir Kleiner, and Erez Hasman

Optical Engineering Laboratory, Faculty of Mechanical Engineering, Technion-Israel Institute of Technology, Haifa 32000, Israel

Received June 17, 2002

Spiral phase elements with topological charges based on space-variant Pancharatnam–Berry phase optical elements are presented. Such elements can be achieved by use of continuous computer-generated space-variant subwavelength dielectric gratings. We present a theoretical analysis and experimentally demonstrate spiral geometrical phases for infrared radiation at a wavelength of 10.6 μm. © 2002 Optical Society of America

OCIS codes: 260.5430, 350.1370, 050.2770, 050.1970.

Recent years have witnessed a growing interest in helical beams that are exploited in a variety of applications. These include trapping of atoms and macroscopic particles,[1,2] transferring of orbital angular momentum to macroscopic objects,[1–3] rotational frequency shifting, the study of optical vortices,[4] and specialized alignment schemes. Beams with helical (or spiral) wave fronts are described by complex amplitudes $u(r, \omega) \propto \exp(-il\omega)$, where r and ω are the cylindrical coordinates, namely, the radial coordinate and the azimuthal angle, respectively, and l is the topological charge of the beams. At the center, the phase has a screw dislocation, also called a phase singularity or optical vortex. Typically, hellical beams are formed by manipulation of light after it emerges from a laser by superposition of two orthogonal (nonhelical) beams or by transformation of Gaussian beams into helical beams by means of computer-generated holograms,[2,4] cylindrical lenses, and spiral phase elements (SPEs).[5] Alternatively, a helical beam can be generated inside a laser cavity by insertion of SPEs into the laser cavity.[6] The common approaches to forming SPEs are as refractive or diffractive optical elements by use of a milling tool, by use of a single-stage etching process with a gray-scale mask, or with a multistage etching process.[6] Such helical beam formations generally are cumbersome or difficult to achieve or suffer from large numbers of aberrations, low efficiency, or large and unstable optical system.

In this Letter we consider novel SPEs based on the space-domain Pancharatnam–Berry phase.[7,8] Unlike diffractive and refractive elements, the phase is not introduced through optical path differences but results from the geometrical phase that accompanies space-variant polarization manipulation. We show that such elements can be achieved by use of continuous computer-generated space-variant subwavelength dielectric gratings. Moreover, we experimentally demonstrate SPEs with different topological charges based on a Pancharatnam–Berry phase manipulation, with axially symmetric local subwavelength groove orientation, for CO_2 laser radiation at a wavelength of 10.6 μm.

Recently, space-variant polarization-state manipulations were demonstrated with computer-generated subwavelength structures.[9] When the period of a subwavelength periodic structure is smaller than the incident wavelength, only zeroth order is a propagating order, and all other orders are evanescent. The subwavelength periodic structure behaves as a uniaxial crystal with the optical axes parallel and perpendicular to the subwavelength grooves. Therefore, by fabricating quasi-periodic subwavelength structures, for which the period and the orientation of the subwavelength grooves were space varying, we achieved continuously rotating wave plates.[10] Furthermore, we showed that such polarization manipulations inevitably lead to phase modification of geometrical origin results from local polarization manipulation and are in fact a manifestation of the geometrical Pancharatnam–Berry phase.[9,11] Optical elements that use this effect to form a desired phase front are called Pancharatnam–Berry phase optical elements (PBOEs).[12] In this Letter we maintain that the formation of a PBOE with a spiral geometrical phase indicates an ability to form complex continuous PBOEs.

The PBOEs are considered wave plates with constant retardation and continuously space varying fast axes, the orientation of which is denoted $\theta(r, \omega)$. It is convenient to describe PBOEs by using Jones calculus. We find the space-dependent transmission matrix for the PBOE by applying the optical rotator matrix to the Jones matrix of the subwavelength dielectric grating to obtain, on a helical basis,[12]

$$\mathbf{T}(r,\omega) = \frac{1}{2}[t_x + t_y \exp(i\phi)]\begin{bmatrix} 1 & 0 \\ 0 & 1 \end{bmatrix} + \frac{1}{2}[t_x - t_y \exp(i\phi)]\begin{bmatrix} 0 & \exp[i2\theta(r,\omega)] \\ \exp[-i2\theta(r,\omega)] & 0 \end{bmatrix}, \quad (1)$$

where t_x and t_y are the real amplitude transmission coefficients for light polarized perpendicular and parallel to the optical axes, respectively, and ϕ is the retardation of the grating. Thus, for an incident plane wave with arbitrary polarization $|\mathbf{E}_{\text{in}}\rangle$, we find that the resulting field is

$$|\mathbf{E}_{\text{out}}\rangle = \sqrt{\eta_E}\,|\mathbf{E}_{\text{in}}\rangle + \sqrt{\eta_R}\exp[i2\theta(r,\omega)]\,|\mathbf{R}\rangle + \sqrt{\eta_L}\exp[-i2\theta(r,\omega)]\,|\mathbf{L}\rangle, \quad (2)$$

0146-9592/02/211875-03$15.00/0

where $\eta_E = |1/2[t_x + t_y \exp(i\phi)]|^2$, $\eta_R = |1/2[t_x - t_y \exp(i\phi)]\langle \mathbf{E}_{\text{in}}|\mathbf{L}\rangle|^2$, and $\eta_L = |1/2[t_x - t_y \exp(i\phi)] \times \langle \mathbf{E}_{\text{in}}|\mathbf{R}\rangle|^2$ are the polarization order coupling efficiencies, $\langle\alpha|\beta\rangle$ denotes an inner product, and $|\mathbf{R}\rangle = (1\ 0)^T$ and $|\mathbf{L}\rangle = (0\ 1)^T$ represent the right-hand and the left-hand circular polarization components, respectively. From Eq. (2) one can see that the emerging beam from a PBOE comprises three polarization orders. The first maintains the original polarization state and phase of the incident beam, the second is right-hand circularly polarized and has a phase modification of $2\theta(r, \omega)$, and the third has a polarization direction and a phase modification opposite those of the former polarization order. Note that the polarization efficiencies depend on the shape and material of the groove as well as on the polarization state of the incident beam. For the substantial case $t_x = t_y = 1$ and $\phi = \pi$, an incident wave with $|\mathbf{R}\rangle$ polarization is subject to total polarization state conversion and results in an emerging field:

$$|\mathbf{E}_{\text{out}}\rangle = \exp[-i2\theta(r, \omega)]\,|\mathbf{L}\rangle\,. \tag{3}$$

An important property of Eq. (3) is that the phase factor depends on the local orientation of the subwavelength grating. This dependence is geometrical in nature and originates solely from local changes in the polarization state of the emerging beam. This dependence can be illustrated by use of a Poincaré sphere with three Stokes parameters, S_1, S_2, and S_3, representing a polarization state, as depicted in Fig. 1(a). The incident right-hand polarized and the transmitted left-hand polarized waves correspond to the north and the south poles of the sphere, respectively. Inasmuch as the subwavelength grating is space varying, the beam at different points traverses different paths on the Poincaré sphere. For instance, the geodesic lines $\hat{A}$ and $\hat{B}$ represent different paths for two waves transmitted through element domains of local orientations $\theta(r, 0)$ and $\theta(r, \omega)$. Geometrical calculations show that the phase difference $\varphi_p = -2\theta(r, \omega)$ between states, corresponding to $\theta(r, 0)$ and $\theta(r, \omega)$ orientations, is equal to half of the area Ω enclosed by geodesic lines $\hat{A}$ and $\hat{B}$.[9,11] This fact is in compliance with the well-known rule, proposed by Pancharatnam, for comparing the phases of two light beams with different polarizations[7] and can be considered an extension into the space domain of the rule that we mentioned.

To design a continuous subwavelength structure with the desired phase modification, we define a space-variant subwavelength grating vector $\mathbf{K}_g(r, \omega)$, oriented perpendicular to the desired subwavelength grooves. Figure 1(b) illustrates this geometrical definition of the grating vector. To design a PBOE with a spiral geometrical phase we need to ensure that the direction of the grating grooves is given by $\theta(r, \omega) = l\omega/2$, where l is the topological charge. Therefore, from Fig. 1(b), the grating vector is given by $\mathbf{K}_g(r, \omega) = K_0(r, \omega)\{\cos[(l/2 - 1)\omega]\hat{r} + \sin[(l/2 - 1)\omega]\hat{\omega}\}$, where $K_0 = 2\pi/\Lambda(r, \omega)$ is the local spatial frequency of a grating with a local period $\Lambda(r, \omega)$.

To ensure the continuity of the subwavelength grooves we required that $\nabla \times \mathbf{K}_g = 0$, which resulted in a differential equation that could be solved to yield the local grating period. The solution to this problem yielded $K_0(r) = (2\pi/\Lambda_0)(r_0/r)^{l/2}$, where Λ_0 is the local subwavelength period at $r = r_0$. Consequently the grating function ϕ_g (defined such that $\mathbf{K}_g = \nabla\phi_g$) was then found by integration of $\mathbf{K}_g(r, \omega)$ over an arbitrary path to yield $\phi_g(r, \omega) = (2\pi r_0/\Lambda_0)(r_0/r)^{l/2-1} \cos[(l/2 - 1)\omega]/(l/2 - 1)$ for $l \neq 2$ and $\phi_g(r, \omega) = (2\pi r_0/\Lambda_0)\ln(r/r_0)$ for $l = 2$. We then obtained a Lee-type binary grating to describe the grating function,[11] ϕ_g, for $l = 1, 2, 3, 4$. The grating was fabricated for CO_2 laser radiation with a wavelength of 10.6 μm, with $\Lambda_0 = 2$ μm, $r_0 = 4.7$ mm, and a maximum radius of 6 mm, resulting in 2 μm $\leq \Lambda(r) \leq$ 3.2 μm. We formed the grating with a maximum local period of 3.2 μm in order not to exceed the Wood anomaly of GaAs. The magnified geometries of the gratings for four topological charges are presented in Fig. 2. The elements were fabricated upon 500-μm-thick GaAs wafers by contact photolithography and electron-cyclotron resonance etching with BCl_3 to a nominal depth of 2.5 μm, resulting in measured values of retardation of $\phi = \pi/2$ and $t_x = t_y = 0.9$. These values are close to the theoretical predictions achieved by rigorous coupled-wave analysis. The inset in Fig. 2 shows

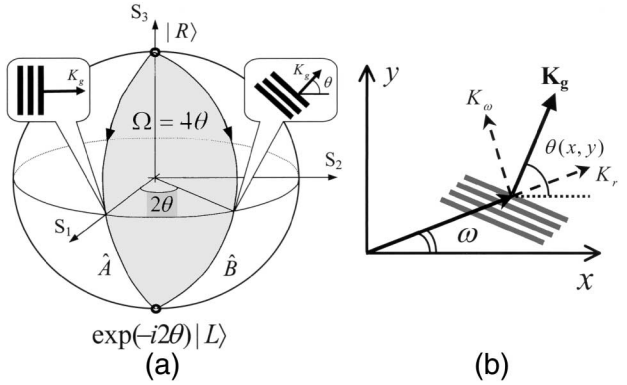

Fig. 1. (a) Illustration of the principle of PBOEs by use of the Poincaré sphere; insets, local orientations of the subwavelength grooves. (b) Geometrical definition of the grating vector.

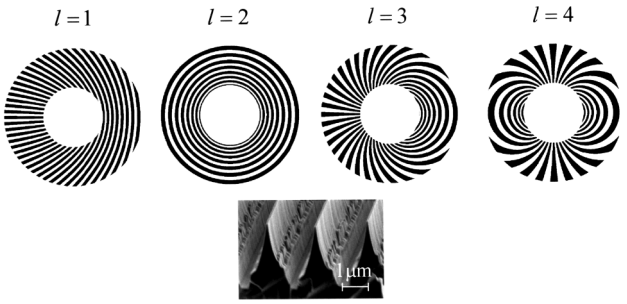

Fig. 2. Top, geometry of the subwavelength gratings for four topological charges. Bottom, image of a typical grating profile taken with a scanning-electron microscope.

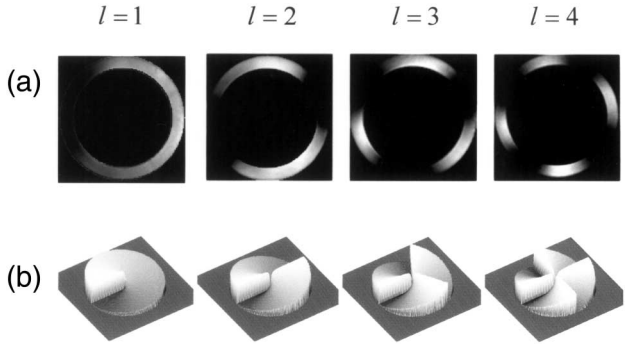

Fig. 3. (a) Interferogram measurements of the spiral PBOEs. (b) The corresponding spiral phases for different topological charges.

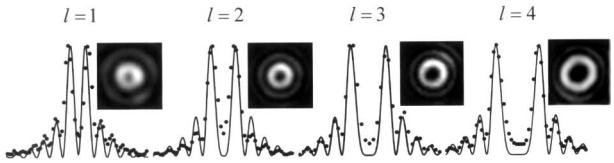

Fig. 4. Experimental far-field images and their calculated and measured cross sections for the helical beams with $l = 1-4$.

a scanning-electron microscope image of one of the dielectric structures.

Following the fabrication, the spiral PBOEs were illuminated with a right-hand circularly polarized beam, $|\mathbf{R}\rangle$, at 10.6-μm wavelength. To provide experimental evidence of the resultant spiral phase modification of our PBOEs we used a self-interferogram measurement, using PBOEs with retardation $\phi = \pi/2$. For such elements the transmitted beam comprises two polarization orders: $|\mathbf{R}\rangle$ polarization state and $|\mathbf{L}\rangle$ with a phase modification of $-il\omega$, according to Eq. (2). The near-field intensity distributions of the transmitted beams that were followed by a linear polarizer were then measured. Figure 3(a) shows the interferogram patterns for various spiral PBOEs. The intensity dependence on the azimuthal angle is of the form $I \propto 1 + \cos(l\omega)$, whereas the number of the fringes is equal to l, the topological charge of the beam. Figure 3(b) illustrates the phase fronts that result from the interferometer analysis, indicating spiral phases with different topological charges.

Figure 4 shows the far-field images of transmitted beams that have various topological charges as well as the measured and theoretically calculated cross sections. We achieved the experimental result by focusing the beam through a 500-mm focal-length lens followed by a circular polarizer. We used the circular polarizer to transmit only the desired $|\mathbf{L}\rangle$ state and to eliminate the $|\mathbf{R}\rangle$ polarization order that appeared because of the insufficient etched depth of the grating. Dark spots can be observed at the center of the far-field images, providing evidence of phase singularity in the center of the helical beams. We found excellent agreement between theory and experiment, clearly indicating the spiral phases of the beams with different topological charges.

To conclude, we have demonstrated the formation of helical beams by using space-variant Pancharatnam–Berry phase optical elements based on computer-generated subwavelength dielectric gratings. The formation of the spiral phase by the PBOE is subject to control of the local orientation of the grating. This can be achieved with a high level of accuracy by use of an advanced photolithographic process. In contrast, in the formation of a SPE based on refractive optics the phase is influenced by fabrication errors caused by inaccuracy of the etched three-dimensional profile. We are currently investigating a photolithographic process with which to achieve accurate control of the retardation phase to yield only the desired polarization order.

E. Hasman's e-mail address is mehasman@tx.technion.ac.il.

References

1. L. Paterson, M. P. MacDonald, J. Arlt, W. Sibbett, P. E. Bryant, and K. Dholakia, Science **292,** 912 (2001).
2. L. Allen, M. J. Padgett, and M. Babiker, in *Progress in Optics*, E. Wolf, ed. (Pergamon, London, 1999), Vol. XXXIX, p. 291.
3. A. Mair, A. Vaziri, G. Weihs, and A. Zeilinger, Nature **412,** 313 (2001).
4. Z. S. Sacks, D. Rozas, and G. A. Swartzlander, Jr., J. Opt. Soc. Am. B **15,** 2226 (1998).
5. M. W. Beijersbergen, R. P. C. Coerwinkel, M. Kristensen, and J. P. Woerdman, Opt. Commun. **112,** 321 (1994).
6. R. Oron, N. Davidson, A. A. Friesem, and E. Hasman, in *Progress in Optics*, E. Wolf, ed. (Pergamon, London, 2001), Vol. XDII, p. 325.
7. S. Pancharatnam, Proc. Ind. Acad. Sci. A **44,** 247 (1956).
8. M. V. Berry, Proc. R. Soc. London Ser. A **392,** 45 (1984).
9. Z. Bomzon, G. Biener, V. Kleiner, and E. Hasman, Opt. Lett. **27,** 285 (2002).
10. Z. Bomzon, A. Niv, G. Biener, V. Kleiner, and E. Hasman, Appl. Phys. Lett. **80,** 3685 (2002).
11. Z. Bomzon, V. Kleiner, and E. Hasman, Opt. Lett. **26,** 1424 (2001).
12. Z. Bomzon, G. Biener, V. Kleiner, and E. Hasman, Opt. Lett. **27,** 1141 (2002).